A reverse Monte Carlo method for deriving optical constants of solids from reflection electron energy-loss spectroscopy spectra

B. Da,[1] Y. Sun,[1] S. F. Mao,[2] Z. M. Zhang,[3] H. Jin,[4] H. Yoshikawa,[4] S. Tanuma,[4] and Z. J. Ding[1,a)]

[1]*Hefei National Laboratory for Physical Sciences at Microscale and Department of Physics, University of Science and Technology of China, 96 Jinzhai Road, Hefei, Anhui 230026, People's Republic of China*
[2]*School of Nuclear Science and Technology, University of Science and Technology of China, 96 Jinzhai Road, Hefei, Anhui 230026, People's Republic of China*
[3]*Centre of Physical Experiments, University of Science and Technology of China, 96 Jinzhai Road, Hefei, Anhui 230026, People's Republic of China*
[4]*Advanced Surface Chemical Analysis Group, National Institute for Materials Science, 1-2-1 Sengen Tsukuba, Ibaraki 305-0047, Japan*

(Received 14 February 2013; accepted 20 May 2013; published online 4 June 2013)

A reverse Monte Carlo (RMC) method is developed to obtain the energy loss function (ELF) and optical constants from a measured reflection electron energy-loss spectroscopy (REELS) spectrum by an iterative Monte Carlo (MC) simulation procedure. The method combines the simulated annealing method, i.e., a Markov chain Monte Carlo (MCMC) sampling of oscillator parameters, surface and bulk excitation weighting factors, and band gap energy, with a conventional MC simulation of electron interaction with solids, which acts as a single step of MCMC sampling in this RMC method. To examine the reliability of this method, we have verified that the output data of the dielectric function are essentially independent of the initial values of the trial parameters, which is a basic property of a MCMC method. The optical constants derived for SiO_2 in the energy loss range of 8-90 eV are in good agreement with other available data, and relevant bulk ELFs are checked by oscillator strength-sum and perfect-screening-sum rules. Our results show that the dielectric function can be obtained by the RMC method even with a wide range of initial trial parameters. The RMC method is thus a general and effective method for determining the optical properties of solids from REELS measurements. © *2013 AIP Publishing LLC*. [http://dx.doi.org/10.1063/1.4809544]

I. INTRODUCTION

Precise information of optical properties for nanostructures and ultrathin films is becoming more important to material science. However, it is still difficult to accurately measure the optical data by optical methods for such nanostructured materials. Fortunately, such information is essentially contained in and, therefore, may be extracted from a surface electron spectroscopy spectrum by using electrons as a probe, like a reflection electron energy loss spectroscopy (REELS) spectrum, due to the shorter information depth of signal electrons compared with that of photons so that the substrate information may be avoided by proper choice of incident angle and energy. REELS then, in principle, provides another means for measuring optical data for solids and thin films.

The interaction process of electrons with a solid and its surface is generally quite complex due to elastic and inelastic collisions. The inelastic interactions are closely related to the optical properties of the sample.[1] Typical inelastic-scattering mechanisms include bulk and surface excitations and interband and intraband transitions. Furthermore, multiple-scattering effects occur because the relevant mean free paths for electron scattering are comparable with or even shorter than the structure feature size.[2–6] Hence, derivation of optical data from REELS spectra requires removing the effects of surface excitations, elastic scattering, and multiple scattering in the data analysis.

The question then arises as to how to extract the single-scattering energy-loss distribution from an experimental REELS spectrum, which is in fact an inverse problem involving many local solutions. Powell performed parametric calculations of the energy-loss function (ELF) for different choices of parameters for the dielectric function;[7] the results of non-linear least square fits of model functions for the dielectric constant to measured optical and energy-loss data were presented for Al between 0.04 and 72 eV (Ref. 8) and for Be, Ge, Sb, and Bi in the vacuum ultraviolet region.[9] These fits as local solutions were imperfect because there were always some small systematic deviations arising from the complex shape of the deviations in multi-parameter space.

Tougaard and Chorkendorff[10] presented a simple deconvolution formula where the physical model is based on the so-called P1-approximation, in which the expansion of the elastic-scattering cross section in spherical harmonics is terminated after the first order.[11] In the medium-energy region, the higher order phase shifts are by no means negligible,[12] and consequently the P1-approximation does not provide a good physical basis to model REELS spectra. Other deconvolution procedure for REELS spectra have been introduced by several authors independently[13–18] in which elastic scattering is treated more realistically. Although these approaches are

a)E-mail: zjding@ustc.edu.cn

better for describing REELS spectra, the surface excitations are still neglected, and the results are quite similar to those obtained using the Tougaard and Chorkendorff algorithm. Recently, Jin *et al.*[19] employed a factor analysis (FA) method to analyze series of spectra for various emission angles at a fixed primary beam energy to separate the surface-loss and bulk-loss components; the optical ELF is then obtained from the extracted bulk-loss components.

Yoshikawa *et al.*[16,20,21] have derived the effective ELF (EELF) from an analysis of a REELS spectrum by incorporating the Landau formulation in a Monte Carlo (MC) simulation of electron trajectories. This EELF obtained is closer to the surface ELF in the low-loss region and to the bulk ELF in the higher energy-loss region and for high-energy electrons. Applying this method, named the extended Landau formulation or the extended Landau approach,[22] Shimizu and coworkers[23–26] have derived the EELF and verified their results by reproducing a REELS spectrum with an early MC simulation using the relevant EELF to replace the optical ELF used conventionally.[27–33] The EELF employed for this MC simulation is in form the same as the bulk ELF while containing contributions from both surface excitations and bulk excitations. The surface excitations by an electron in the vicinity of a surface are thus treated as depth-independent events in the same way as bulk excitations. However, because this is an over-simplified treatment for surface excitations, there were still discrepancies between simulated and experimental data.

Recently, Yoshikawa *et al.*[34] have made drastic improvements in their target factor analysis (TFA) method. Bulk ELFs can be separated from the surface-loss structures of REELS spectra. This improved method for determining the bulk ELFs is largely unaffected by the condition of the outermost surface layers. Therefore, this method will be particularly useful for analysis of dielectric properties of compounds and oxides for which it is difficult to produce a clean surface without destroying the structure and composition of the outermost few atomic layers. However, artificial judging and limitations are still necessary in this method.

Recently, Werner presented a procedure to decompose experimental REELS spectra of medium-energy electrons reflected from solid surfaces into contributions due to surface and bulk electronic excitations.[35,36] The procedure is based on the simultaneous deconvolution of a set of two REELS spectra taken at different energies or geometrical configurations for which the relative contribution of surface excitation to bulk excitation differs substantially. The main assumption in this procedure is that the surface and bulk excitations for inelastic scattering can be treated as separate events.[37] An example was given for Au where two sets of REELS spectra taken at different energies above 1000 eV, where the influence of the surface is less critical, were shown to give similar results.[38] Based on this deconvolution method, Werner *et al.*[39] have built a database of optical constants for 16 elemental metals (Ti, V, Fe, Co, Ni, Cu, Zn, Mo, Pd, Ag, Ta, W, Pt, Au, Pb, and Bi) and one semimetal (Te) from measured REELS spectra as well as density functional theory (DFT) calculations. For use of REELS to study the dielectric properties of nanostructures or ultrathin films, however, it is necessary to consider low primary energies.

Due to complicated electron-transport processes, the ELF is involved in a measured REELS spectrum in a more complex way other than simple convolutions. Obtaining the desired optical data from a measured spectrum is an inverse problem and it is generally hard to develop a suitable mathematical formalism to ensure good accuracy and computational efficiency. In the present work, we have developed a new method, the reverse Monte Carlo (RMC) method, to solve the inverse problem by taking advantage of the well developed MC technique for simulation of REELS spectra. For a description of a REELS spectrum, the MC method exceeds any analytical deconvolution method. The problem becomes how to efficiently and automatically deduce an ELF in a calculation algorithm with less manual intervention. The principle of this RMC method is based on an iterative process of improving oscillator parameters by minimizing the differences between a simulated and a measured REELS spectrum. The EELF can be expressed as a linear combination of bulk ELF and surface ELF contributions. This test EELF is then employed in a MC simulation of electron interactions with the sample; by comparing the simulated REELS spectrum with an experimental spectrum, we can estimate the precision of oscillator parameters, weighting factors for the surface and bulk excitations contribution and the band gap energy for non-conductors. Depending on differences between measured and simulated REELS spectra, the EELF is updated by modifying oscillator parameters, weighting factors, and the band gap energy, and the process is repeated until the differences are negligible.

Since there are many parameters, the problem is actually global optimization. In this RMC method, it is important to minimize the computation time for deriving the best set of fitted parameters. This is done by using a Markov chain Monte Carlo (MCMC) sampling procedure, i.e., Metropolis importance sampling, for adjusting the parameter set. The Metropolis-Hastings algorithm[40,41] is the most popular MCMC method that is widely used in statistical physics for efficient random sampling of a probability distribution, e.g., high-dimensional probability distributions, for which direct sampling is difficult. Because the number of parameters involved in describing EELF is often quite large, for describing complex electronic excitations in a REELS spectrum, a simulated annealing method is adopted to find the minimum "potential energy" corresponding to the best fitted-parameter set in the high-dimensional parameter space. Simulated annealing[42,43] is a random-search technique which exploits an analogy between the way in which a metal slowly cools down and freezes into the minimum energy crystalline structure (the annealing process). The search for a minimum in a more general system forms the basis of an optimization technique for combinatorial and other problems.

By combining a well developed MC simulation method for electron-solid interactions with MCMC estimation of oscillator parameters, our new theoretical RMC method for extraction of the optical properties of bulk materials from measured REELS spectra is expected to show both good accuracy and good efficiency. As an example, the bulk ELF

and optical constants of SiO_2 are successfully obtained from measured REELS spectra. A basic property of the MCMC method is that the equilibrium state is independent of the initial state of a Markov chain; that is, the final output of the best-fitted parameter set does not depend on the initial values of the trial parameters. To verify this, we have compared the computed ELFs of SiO_2 obtained with different initial oscillator parameters as inputs; this comparison showed that the final ELFs with different initial values agreed reasonably with each other.

II. EXPERIMENTAL

A SiO_2 film with thickness of 100 nm was grown on a Si substrate by thermal oxidation. Before measuring the REELS spectra, the SiO_2 specimen was thermally annealed at 400 °C for 5 h in a furnace to remove surface contamination.[44,45] A very small amount of carbon was detected by AES at higher emission angles after this effective cleaning treatment. REELS experiments at various emission angles were carried out with an inclined sample holder. Fig. 1 shows the configuration for the REELS experiments. A sample was mounted on a sample holder which is inclined by 30°. This setup can provide a wide range of emission angles to the surface normal (15°–75°) by rotating the sample holder. The electron-gun axis is in the vertical direction and on the rotation axis of the sample holder. This configuration gives a constant incidence angle of 30° with respect to the surface normal. The angle between the axis of the electron-gun and the analyzer is 45°. The REELS spectra were measured using the Ulvac-Phi model 5500 electron spectrometer equipped with a concentric hemispherical analyzer which was modified to analyze high kinetic energy electrons up to 4800 eV. We obtained a series of spectra with different emission angles at fixed primary beam energy. The spectra were measured in the constant analyzer energy mode with 23.5 eV pass energy, and data were acquired with a 0.1 eV energy step. The pressure in the analysis chamber was $<2.7 \times 10^{-7}$ Pa.

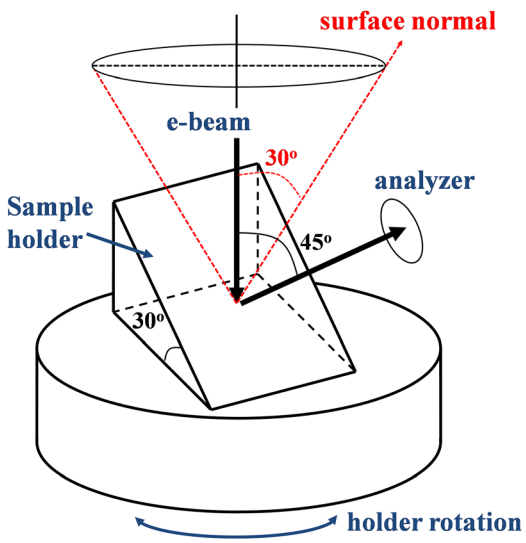

FIG. 1. Configuration for REELS experiments.

III. THEORETICAL

The RMC method developed in this work to deduce bulk ELFs from measured REELS data is an iterative MC simulation process, which is schematically shown in Fig. 2. In each iterative step, or a single step of a MCMC, a MC simulation of a REELS spectrum is performed based on the inelastic-scattering cross-section calculated by using a bulk ELF with newly updated oscillator parameters, weighting factors, and band-gap energy. Although the final ELF from the MCMC output is independent of initial values of parameter set, the proper choice of the trial input values can accelerate the convergence of the parameter set in the MCMC procedure. Therefore, instead of deciding initial parameters arbitrarily, we determined them partly from the calculated band structure and total density of states (DOS). The surface and bulk excitation weighting factors can also be initially estimated by an equation. Then the test ELF is employed in a MC simulation of electron interactions with the sample, and we estimate its accuracy by comparing a simulated REELS spectrum with the experimental spectrum. From differences in these spectra the ELF is updated by the Metropolis importance sampling method to obtain a new parameter set, whose equilibrium value would, in principle, be optimal when the differences are minimized. In short, the principle of this RMC method is to choose efficiently the best-fit ELF which can produce a MC-simulated REELS spectrum with smallest differences to the measured spectrum, from numerous trials of possible ELFs. The problem reduces to finding the global minimum of the potential-energy surface in multi-parameter space, which is approached by simulated annealing.

A. Physical model for MC simulation

The main features of the physical model for MC simulation of electron-solid interaction to produce a REELS spectrum are the use of Mott cross sections for describing electron elastic scattering and a dielectric model for electron inelastic scattering.

The relativistic expression for electron-atom scattering, the Mott differential cross section,[46] is given by

$$\frac{d\sigma}{d\Omega} = |f(\vartheta)|^2 + |g(\vartheta)|^2, \tag{1}$$

with the scattering amplitudes calculated by the partial-wave expansion method[47]

$$f(\vartheta) = \frac{1}{2iK}\sum_{\ell=0}^{\infty}\{(\ell+1)(e^{2i\delta_\ell^+}-1) + l(e^{2i\delta_\ell^-}-1)\}P_\ell(\cos\vartheta),$$
$$g(\vartheta) = \frac{1}{2iK}\sum_{\ell=1}^{\infty}\{-e^{2i\delta_\ell^+} + e^{2i\delta_\ell^-}\}P_\ell^1(\cos\vartheta). \tag{2}$$

In the above equation $P_\ell(\cos\vartheta)$ and $P_\ell^1(\cos\vartheta)$ are, respectively, the Legendre and the first-order associated Legendre functions. δ_ℓ^+ and δ_ℓ^- are spin-up and spin-down phase shifts of the ℓth partial wave. The phase shifts are numerically evaluated by solving the Dirac equation for the radial part of the wave function of the scattered electron. The

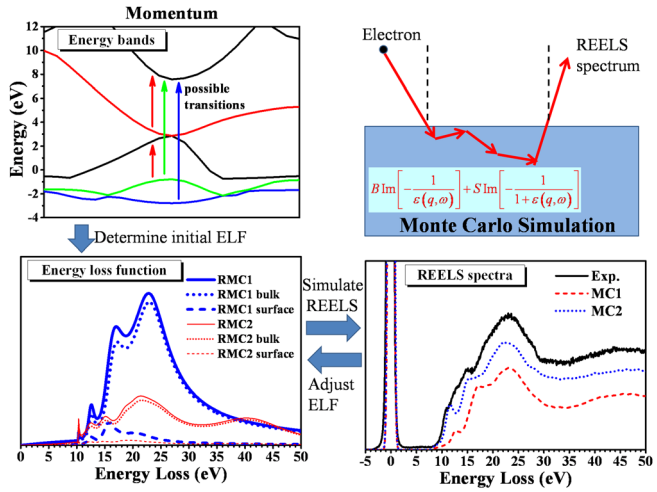

FIG. 2. Diagram of simplified process of forming a REELS spectrum, Monte Carlo process, and a schematic diagram of the RMC process to deduce the bulk ELF from a measured REELS spectrum. The top left figure is a diagram of the calculated SiO_2 band structure; the top right figure shows the MC simulation procedure based on electron inelastic scattering simplified with EELF; the bottom left figure shows EELFs for any two different iteration steps together with the corresponding surface and bulk ELFs; the bottom right figure shows REELS spectra performed by MC simulations for two different iteration steps.

Thomas-Fermi-Dirac (TFD) atomic potential[48] is used in the calculation. We note that differential elastic-scattering cross sections obtained from the Dirac-Hartree-Fock (DHF) potential[49] agree better with measured cross section than those from the TFD potential. However, the difference from using TFD and DHF potentials is small for light elements, such as O and Si, at primary electron energies higher than 1 keV.[50]

The differential inelastic mean free path in the surface region of a solid is represented in dielectric theory in terms of bulk ELF, $\mathrm{Im}\{-1/\varepsilon(q,\omega)\}\Theta(\hbar\omega - E_g)$, and the surface ELF, $\mathrm{Im}\{-1/(1+\varepsilon(q,\omega))\}\Theta(\hbar\omega - E_g)$.[51–53] Here, for simplicity, the EELF is approximated as a linear combination of these ELFs

$$\frac{d^2\lambda_{in}^{-1}}{d(\hbar\omega)dq} = \frac{1}{\pi a_0 E}\left(B\,\mathrm{Im}\left\{\frac{-1}{\varepsilon(q,\omega)}\right\} + S\,\mathrm{Im}\left\{\frac{-1}{1+\varepsilon(q,\omega)}\right\}\right) \times \frac{1}{q}\Theta(\hbar\omega - E_g), \tag{3}$$

where $\hbar\omega$ and $\hbar q$ are the energy loss and the momentum transfer, respectively, from an electron of kinetic energy E penetrating into a solid of dielectric function, $\varepsilon(q,\omega)$. λ_{in} is the electron inelastic mean free path (IMFP), $\Theta(\hbar\omega - E_g)$ is the Heaviside step function, and E_g is the band gap energy. B and S are, respectively, weighting factors for the bulk and surface contributions.[18,54–56] The bulk ELF usually considered in the representation of the differential inelastic mean free path is now replaced by the EELF to take into account surface excitations. This approach allows much faster calculation of the differential inelastic mean free path in updating a MCMC step and is simpler than other more complex formulations involving quantum[51–53] or semi-classical schemes.[57–60]

The weighting factors can be roughly estimated by an empirical equation as

$$B = \frac{\int_d^\infty dz \exp\left(-\frac{z}{\lambda_{in}\cos\alpha} - \frac{z}{\lambda_{in}\cos\theta}\right)}{\int_0^\infty dz \exp\left(-\frac{z}{\lambda_{in}\cos\alpha} - \frac{z}{\lambda_{in}\cos\theta}\right)} = \exp\left(-\frac{d(\cos\alpha+\cos\theta)}{\lambda_{in}\cos\alpha\cos\theta}\right),$$
$$S = \frac{\int_0^d dz \exp\left(-\frac{z}{\lambda_{in}\cos\alpha} - \frac{z}{\lambda_{in}\cos\theta}\right)}{\int_0^\infty dz \exp\left(-\frac{z}{\lambda_{in}\cos\alpha} - \frac{z}{\lambda_{in}\cos\theta}\right)} = 1 - B, \tag{4}$$

where z is the depth coordinate perpendicular to the sample surface and d is a phenomenological parameter characterizing the thickness of the sample region where surface excitations dominate and whose value is of the same order of magnitude as the wavelength of the primary electrons. The incidence angle, α, and emission angle, θ, are measured with respect to the surface normal. $(\cos\alpha + \cos\theta)/\lambda_{in}\cos\alpha\cos\theta$ is an effective penetration depth of the electrons without signal attenuation due to inelastic scattering in the bulk material.

The dielectric function, $\varepsilon(q,\omega)$, may be derived from optical constants either from the plasmon-pole approximation[61] or from Ritchie and Howie's scheme[62] in which an extrapolation from the optical limit ($q = 0$) to other momentum transfers can be made. $\varepsilon(q,\omega)$ is thus approximately extended from an optical dielectric function, $\varepsilon(\omega)$. In our calculation, Ritchie and Howie's scheme[62] is employed.

For many materials, such as SiO_2 with the complex band structure shown in Fig. 3, interband transitions can be incorporated into the Drude model by adding the subband electrons to the free-electron system; the oscillators composing the dielectric function are each characterized by three parameters: the oscillator strength, a_i, damping constant, γ_i, and critical-point energy, ω_i. Based on the superposition of damped linear oscillators, one can write the imaginary and real parts of the dielectric function as, respectively,[63]

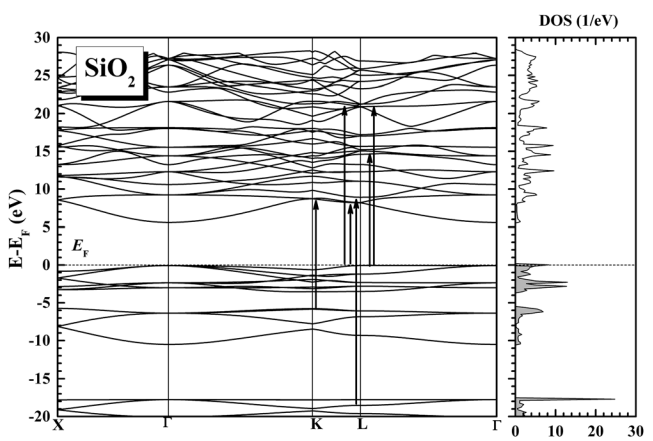

FIG. 3. Calculated band structure (left) and total DOS (right) of bulk β-Cristobalite (cubic) in the energy range from −20 to 30 eV. The Fermi energy is set to zero.

$$\varepsilon_2(0,\omega) = \sum_i \frac{a_i \gamma_i \omega}{(\omega^2 - {\omega_i}^2) + \omega^2 {\gamma_i}^2} \tag{5}$$

and

$$\varepsilon_1(0,\omega) = \varepsilon_B - \sum_i \frac{a_i(\omega^2 - {\omega_i}^2)}{(\omega^2 - {\omega_i}^2) + \omega^2 {\gamma_i}^2}, \tag{6}$$

where ε_B is the background value of the dielectric function. In this work, the optical dielectric function is constructed with N oscillator terms with $3N + 1$ parameters.

B. Algorithm of RMC procedure

The iterative process in this RMC method employs a standard MCMC procedure[40,41,64] and simulated annealing[42,43] to update these parameters efficiently. The algorithm is as follows:

(1) The initial $3(N + 1)$ parameter set, including the $3N + 1$ oscillator parameters (a_i, ω_i, γ_i, ε_B), bulk and surface weighting factors (B, $S = 1 - B$), and the band gap energy (E_g), can be chosen as arbitrary positive numbers, but this would result in a much longer convergence time. We start with parameters partly deduced from first-principles calculation: a_i and γ_i are simply set at random while the initial ω_i parameters and the initial E_g are determined from the calculated energy bands and total DOS. The initial B and S are estimated from Eq. (4).

(2) Based on this dielectric function, a Monte Carlo simulation is performed to obtain the REELS spectrum, $I_0^{\text{sim}}(\Delta E_j)$, where the index j denotes the jth experimental grid value of energy loss ΔE. The simulation procedure is the same as previously published[27,28] except the simulation model for electron inelastic scattering is given by Eq. (3).

(3) Calculate the sum of least-squares relative differences between the experimental REELS spectrum, $I^{\text{exp}}(\Delta E_j)$, and the MC simulated spectrum, $I_0^{\text{sim}}(\Delta E_j)$,

$$\chi_0^2 = \sum_j (I_0^{\text{sim}}(\Delta E_j) - I^{\text{exp}}(\Delta E_j))^2 / \sigma(\Delta E_j)^2, \tag{7}$$

where the summation is taken over the experimental grid values of energy loss. $\sigma(\Delta E_j)$ is the artificially specified weighting-factor spectrum whose relative value emphasizes the energy-loss region of importance in optimization while the absolute value represents the meaning of "temperature" in simulated annealing. Initial values of $\sigma(\Delta E_j)$ for various energies are set as $10 \times |I_0^{\text{sim}}(\Delta E_j) - I^{\text{exp}}(\Delta E_j)|$. Each χ^2 value defines the "potential energy" to be minimized in a MCMC simulation.

(4) By adjusting one parameter among the $3(N + 1)$ parameter set, such as the ith oscillator strength, at random in a specified range, a new dielectric function and hence, bulk ELF and surface ELF, are obtained; then we perform a new MC simulation of a REELS spectrum to derive the updated spectrum, $I_1^{\text{sim}}(\Delta E_j)$. This step produces a new "potential energy"

$$\chi_1^2 = \sum_j (I_1^{\text{sim}}(\Delta E_j) - I^{\text{exp}}(\Delta E_j))^2 / \sigma(\Delta E_j)^2. \tag{8}$$

(5) Calculate change of potential energy in this MCMC step, $\Delta\chi_1^2 = \chi_1^2 - \chi_0^2$. If $\Delta\chi_1^2 < 0$, the move is accepted and the dielectric function is updated; If $\Delta\chi_1^2 > 0$, then the move is accepted only with the probability, $\exp(-\chi_1^2)/\exp(-\chi_0^2) = \exp\{-(\chi_1^2 - \chi_0^2)\}$, according to Metropolis importance sampling[42,43] where the "temperature" factor in a Boltzmann distribution has already been included in $\sigma(\Delta E_j)$ as its absolute value; otherwise, the move is rejected, and we repeat step 4 by adjusting another oscillator parameter.

(6) Repeat steps 4 and 5 for the next iteration. Successive iterations generate decreasing values of potential energy χ_n^2 until they reach a minimum value with only slight fluctuation.

(7) Decrease the absolute value of $\sigma(\Delta E_j)$ by a certain amount and repeat steps 3–6. The temperature factor $\sigma(\Delta E_j)$ proportional to $|I^{\text{sim}}(\Delta E_j) - I^{\text{exp}}(\Delta E_j)|$ plays a crucial role in controlling the evolution of the $3(N + 1)$ parameters: with larger $\sigma(\Delta E_j)$ values the evolution of these parameters is sensitive to coarser spectrum differences, and to finer differences when $\sigma(\Delta E_j)$ is small. In the final stage, this factor is set as a constant. This simulated annealing procedure from high temperature down to low temperature can, in principle, help to find the global minimum potential energy rather than the local minimum in multi-parameter space. The simulated annealing for converging $\Delta\chi_n^2$ finally leads to an equilibrium macrostate composed of many microstates, each of which is specified by a single set of oscillator parameters, around the global minimum energy in multi-parameter space, where the differences between a simulated REELS spectrum and the measured spectrum become negligible.

This RMC simulation procedure can thus automatically optimize the dielectric function to obtain the smallest difference between the simulated and measured REELS data. It is particularly important that this RMC uses the MCMC principle to accelerate the global optimization of the parameter set. In addition the final result should become independent of the initial values for each parameter.

IV. RESULTS AND DISCUSSION

The calculated band structure and total density of states of bulk β-Cristobalite (cubic) in the energy range -20 to 30 eV by the DFT-LDA method (where LDA stands for local-density approximation) is presented in Fig. 3. The highest valence bands, clustered around -1 eV, are derived from the oxygen lone-pair orbitals,[65–67] oxygen p states oriented perpendicular to the Si-O-Si axis. The next set of bands, from -5 to -10 eV, represents the Si-O bonding states. They involve mostly silicon s orbitals and oxygen and silicon p orbitals pointing along the Si-O-Si axes. Finally, the $\sim$2 eV wide bands around -19 eV are derived mostly from oxygen 2 s.[68] The lowest conduction bands due to the atomic silicon 3 s-3 p splitting[69] cluster around $\sim$9 eV, and

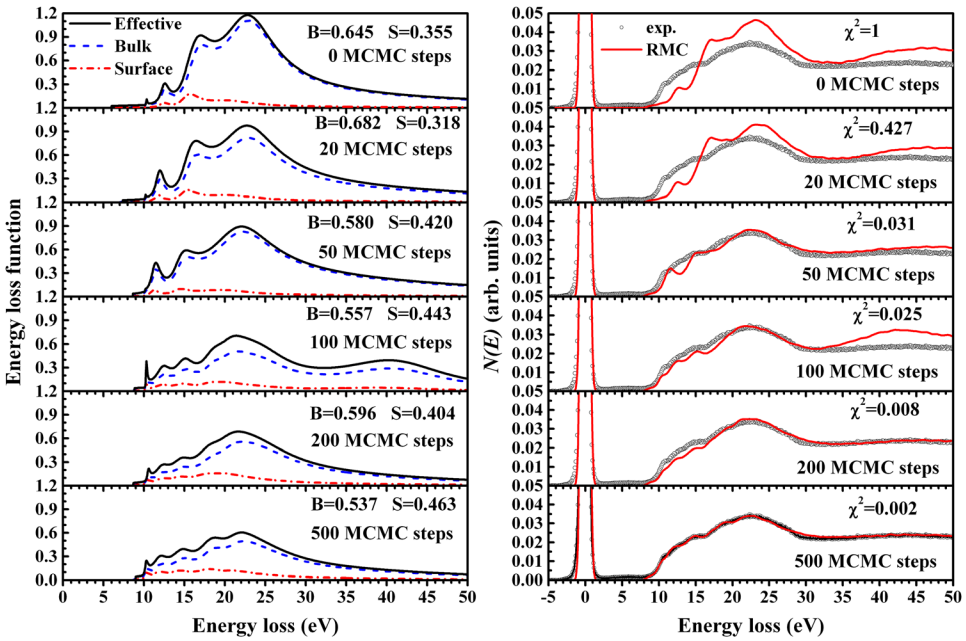

FIG. 4. The updating process of oscillator parameters and weighting factors in the RMC process to derive EELF (left) (EELF is defined as $B\times\mathrm{Im}\{-1/\varepsilon\ (q,\omega)\}+S\times\mathrm{Im}\{-1/(1+\varepsilon(q,\omega))\}$, where $B\times\mathrm{Im}\{-1/\varepsilon(q,\omega)\}$ is the bulk ELF and $S\times\mathrm{Im}\{-1/(1+\varepsilon(q,\omega))\}$ is the surface ELF). The resulting simulated REELS spectrum is compared with an experimental spectrum (right), where $\chi^2=\sum_j\{(I^{\mathrm{sim}}(\Delta E_j)-I^{\mathrm{exp}}(\Delta E_j))/I^{\mathrm{exp}}(\Delta E_j)\}^2$.

the minimum is ~6 eV. Therefore, the computed band gap is ~6 eV, which is smaller than the value 9.0 eV found from photoconductivity measurements.[70] The DFT-LDA method gives rise to good structural parameters but fails to describe the fundamental gap energies especially for semiconductors.[71,72] Some of the possible transitions from occupied bands into unoccupied bands are also drawn in Fig. 3. From various possible excitations, initial values for the critical-point energies of the seven oscillators are chosen as 7, 10, 12, 14, 17, 23, and 35 eV. The background value of the dielectric function ε_B is set at 1, and the corresponding strengths and damping constants of the oscillators are set randomly. We use Eq. (4) to estimate the initial bulk and surface weighting factors at different primary electron energies and geometrical configurations in a REELS experiment.

Using these initial parameters, the RMC procedures are performed for SiO_2 and at electron energies of 2000, 3000, and 4000 eV. The incident angle is fixed at 30°, and the emission angle varies in a range 15°–75° to the surface normal, while the angle between the axis of the electron-gun and the analyzer is 45°. Fig. 4 shows an example of updating the EELF and the resulting simulated REELS spectrum in a RMC process. The calculation time to obtain satisfactory convergence is about 100 h with one CPU (Intel Xeon E7540 running at 2.0 GHz). The changing of values for the least-squares χ^2 with each MCMC step is also given. Fig. 5 shows the final simulated REELS spectra of SiO_2 together with experimental spectra at emission angles of 15°, 30°, 48°, 56°, 64°, 70°, and 75°, for primary electron energies of 2000, 3000, and 4000 eV. It is obvious that the final simulated REELS spectra fit with the experimental spectra very well, especially in the low-energy loss region due to use of relative differences in the RMC procedure using $\sigma(\Delta E_j)$ in Eq. (7).

Bulk ELFs, $\mathrm{Im}\{-1/\varepsilon(q,\omega)\}$, obtained from RMC simulations of experimental REELS spectra are shown in Fig. 6. One can clearly see a strong loss peak at ~23 eV which dominates the bulk ELFs. Some weak peaks occur at ~11, 12, 16, and 18 eV that correspond to interband transitions. We also see a remnant of the surface plasmon feature on the lower energy side of the main peak. Because we have used a simple surface ELF, $\mathrm{Im}\{-1/(1+\varepsilon(q,\omega))\}$, to describe surface excitations by Eq. (3), the surface-excitation feature may still be present to a small extent in the bulk ELF. Because the Begrenzungs effect is important for semiconductors, such as SiO2, especially at small crossing angles,[73] not only the increase of surface excitations but also reduction of volume excitations is significant in this surface-excitation feature. Therefore, the intensity of this peak increases slightly at larger emission angles where stronger surface excitation is expected; meanwhile, the intensity of the bulk excitation peak at ~23 eV gradually decreases. Such small variations of the obtained bulk ELFs with primary energy and emission angle are likely due to the Begrenzungs effect, as found by others.[19,74] In our MC simulation the assumption was made that the probability of surface excitation is independent of the depth underneath the surface. However, with increasing depth the probability of exciting a surface plasmon decreases, and the relative probability of exciting a bulk plasmon increases. Therefore, with the different probing depths for varied varying emission angles, the relative peak intensities for various coupling of surface- and bulk-plasmon excitations will change. This explains the reduction of intensity for the bulk excitation shoulder in the range of 30–60 eV on the higher-energy side of the main peak with increasing emission angle.

The final bulk weighting factors and the band gap energy together with corresponding error ranges are shown in Fig. 7. Here, the usual thermal equilibrium averaging over microstates has not been taken, but only the output data for the last microstate is shown. It is obvious that the bulk weighting factor B decreases with increasing emission angle and decreasing primary energy, due to the enhancement of surface excitations. The precision of the band gap energy E_g obtained in the RMC method is primarily determined by noise in the measured REELS spectra. The error ranges in the figure are determined by the maximum and the minimum values of obtained E_g values in all MCMC steps when the

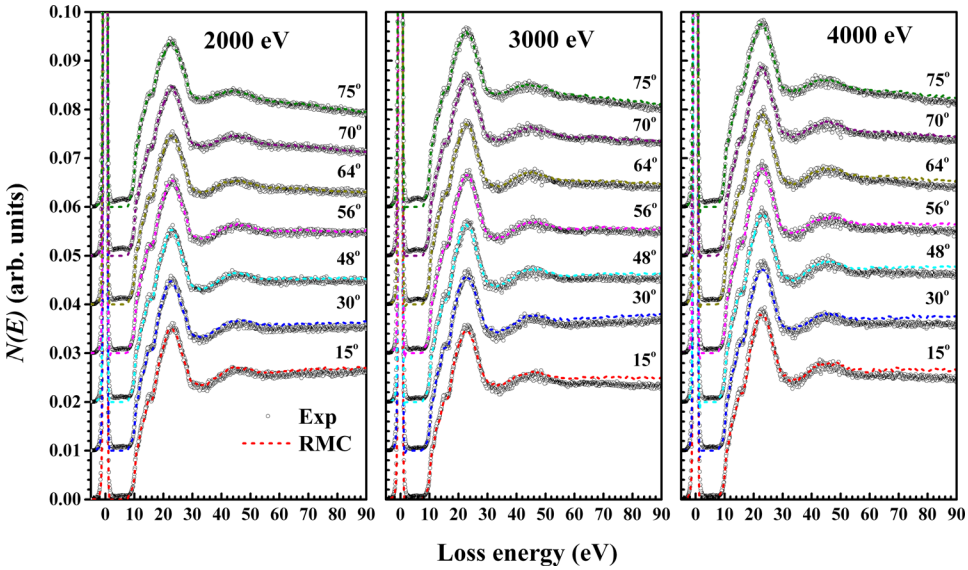

FIG. 5. Comparison of the final simulated REELS spectra of SiO_2 (dashed curve) with the measured REELS spectra[19] (open circles) at various emission angles for primary electron energies of 2000, 3000, and 4000 eV.

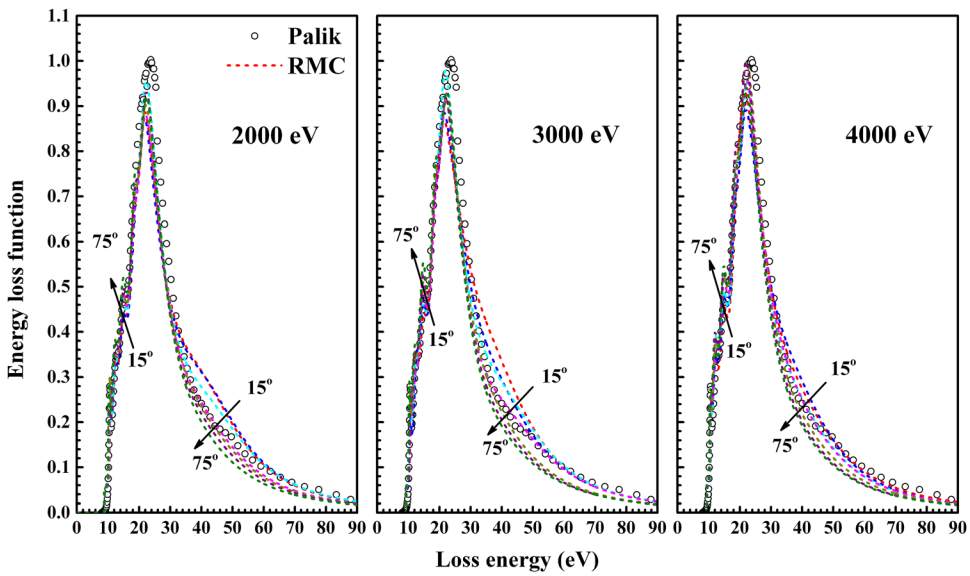

FIG. 6. Final bulk ELFs (dashed curves) of SiO_2 obtained from the RMC simulation of experimental REELS spectra at various emission angles for primary electron energies of 2000, 3000, and 4000 eV in Fig. 5. Palik's data obtained by optical methods (open circles) are also shown as reference values.

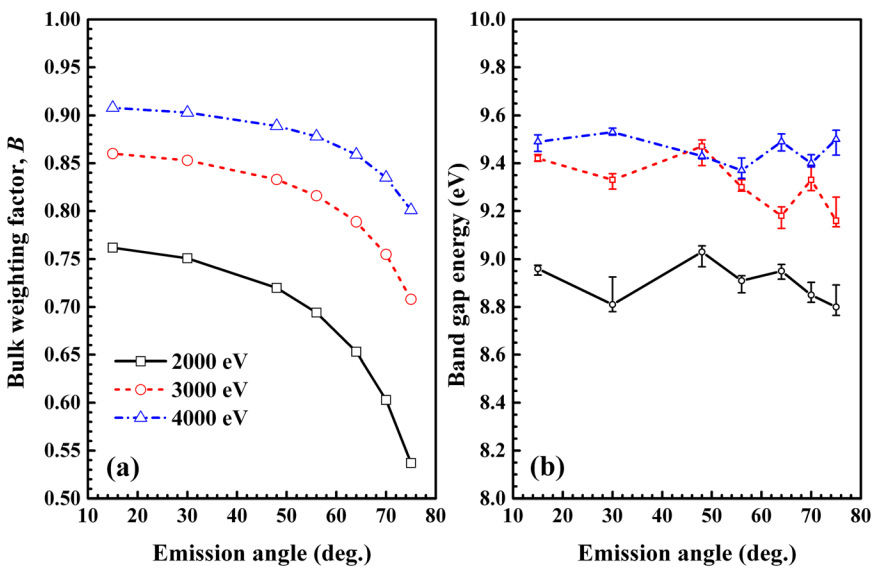

FIG. 7. (a) Plots of the final bulk weighting factor B and (b) the final band gap energy E_g from the RMC procedure at various emission angles for primary electrons with energies of 2000 (open squares), 3000 (open circles), and 4000 eV (open triangles) together with corresponding error ranges. The error ranges are determined from the maximum and the minimum values of obtained E_g values in all MCMC steps when the deviation becomes stable after about 1500 accepted steps.

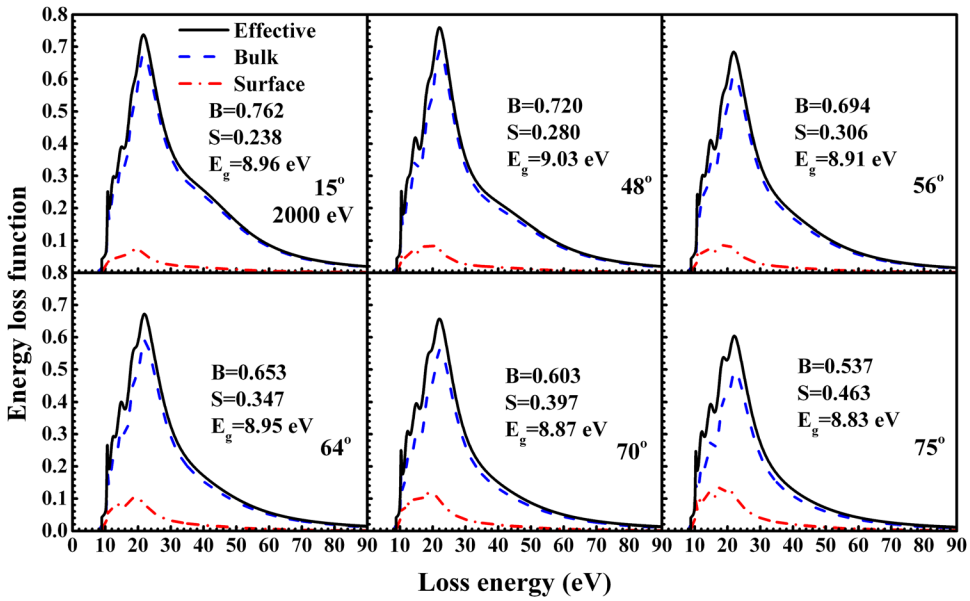

FIG. 8. Results of the EELFs of SiO_2 at various emission angles for 2000 eV electrons by the RMC method (solid curve). The EELF is a linear combination of the surface (dashed dotted curve) and the bulk loss (dashed curve) components, where the EELF is defined as $B\times\mathrm{Im}\{-1/\varepsilon(q,\omega)\}+S\times\mathrm{Im}\{-1/(1+\varepsilon(q,\omega))\}$, the bulk ELF is $B\times\mathrm{Im}\{-1/\varepsilon(q,\omega)\}$, and the surface ELF is $S\times\mathrm{Im}\{-1/(1+\varepsilon(q,\omega))\}$.

deviation becomes stable after about 1500 accepted steps. For primary energies of 2000, 3000, and 4000 eV, the mean value of E_g is about 9.2 eV in accord with experimental results, 9.0 eV in Ref. 70 and 9.2 eV in Ref. 75. From a linear combination of the surface ELF and bulk ELF components, the EELFs of SiO_2 at emission angles of 15°, 48°, 56°, 64°, 70°, and 75°, for 2000 eV electrons are illustrated in Fig. 8. It is clear that the relative magnitudes of surface-loss and bulk-loss components depend on the emission angle.

In order to assess the reliability of the RMC method, we have performed tests in which different initial input parameters are used in simulations for the same experimental REELS spectrum. Fig. 9 shows that the relatively large uncertainty ranges for $\varepsilon_2(\omega)$ and $\mathrm{Im}\{-1/\varepsilon(\omega)\}$, which are obtained from their maximum and the minimum values for eight different initial parameter sets. The inputs for the trial oscillator parameters, weighting factor, and band gap energy were determined randomly. By using these different initial parameter sets in the RMC simulation, the final results for $\varepsilon_2(\omega)$ and $\mathrm{Im}\{-1/\varepsilon(\omega)\}$ after about 1500 accepted MCMC steps are shown in Fig. 10. Palik's data from optical measurements[76] are also presented for comparison. It is obvious that all the final results with different inputs do converge; the consistency is also found to be

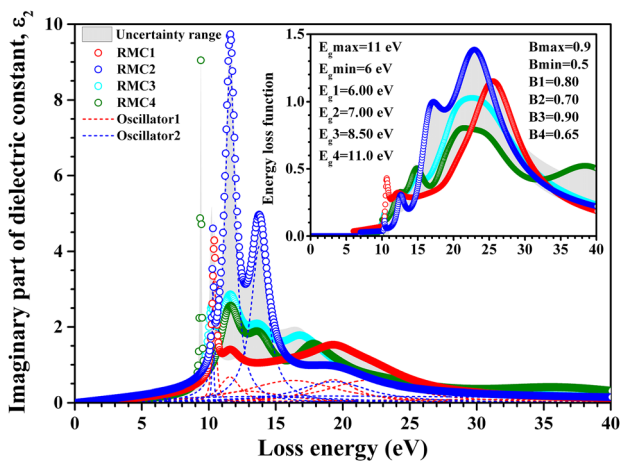

FIG. 9. A plot of uncertainty ranges for the initial imaginary part of dielectric constant, $\varepsilon_2(\omega)$ (gray area), resulting from choices of eight different initial oscillator parameter sets as inputs for RMC simulations. Four of these inputs are shown (open circles). The initial band-gap energy of eight inputs are chosen as 6.0 eV (RMC1), 7.0 eV (RMC2), 8.0 eV, 8.5 eV (RMC3), 9.0 eV, 9.5 eV, 10.0 eV, and 11.0 eV (RMC4), and the initial bulk weighting factors are chosen as 0.8 eV (RMC1), 0.7 eV (RMC2), 0.8 eV, 0.9 eV (RMC3), 0.5 eV, 0.55 eV, 0.6 eV, and 0.65 eV (RMC4). For clarity, only two sets of oscillator components are illustrated (dashed curves). The inset shows the uncertainty range of the corresponding bulk ELFs (shading area), together with four initial bulk ELFs (open circles), and the initial bulk weighting factors and band gap energies.

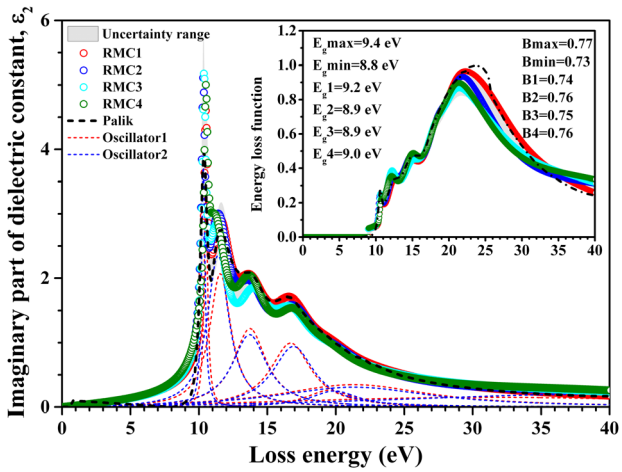

FIG. 10. A plot of uncertainty range for the final output of the imaginary part of dielectric constant, $\varepsilon_2(\omega)$ (shaded area), after RMC simulations with the eight different sets of initial parameters shown in Fig. 9. Four of the eight outputs are shown (open circles). The final band-gap energy of eight outputs are 9.2 eV (RMC1), 8.9 eV (RMC2), 8.8 eV, 8.9 eV (RMC3), 9.0 eV, 9.1 eV, 9.4 eV, and 9.0 eV (RMC4), and the final bulk weighting factors are 0.74 eV (RMC1), 0.76 eV (RMC2), 0.74 eV, 0.75 eV (RMC3), 0.73 eV, 0.73 eV, 0.77 eV, and 0.76 eV (RMC4). For clarity, only two sets of oscillator components are illustrated (dashed curves). The inset shows the uncertainty range of the corresponding bulk ELFs (shaded area) together with four final bulk ELFs (open circles), and the final values of the bulk weighting factors and band gap energies. Palik's data (long dashed curve) are shown for comparison.

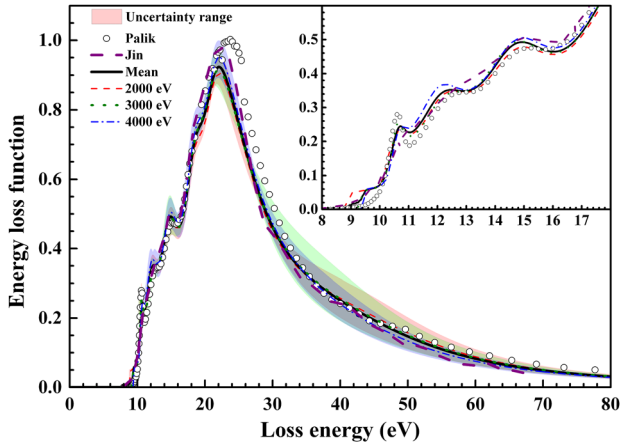

FIG. 11. Bulk ELFs of SiO_2 obtained for 2000, 3000, and 4000 eV electrons by the RMC method together with the uncertainty range (shaded area). The mean value of the bulk ELF (thick curve), Jin's data[19] deduced from the same REELS spectra, and Palik's data are also presented. The inset shows the bulk ELF in the low energy-loss region.

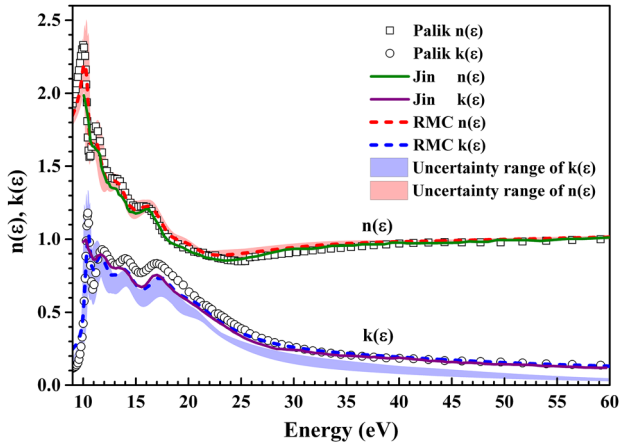

FIG. 12. The calculated refractive index n (dashed curve) and extinction coefficient k (dashed curve) of SiO_2 by using RMC method together with corresponding uncertainty range (shaded area). As a reference, Jin's data[19] from the same measured REELS spectra (solid curves) and the Palik's data (open squares and circles) are also shown.

excellent in the low-energy loss region because of our use of relative differences in the RMC procedure. All of the obtained $\varepsilon_2(\omega)$ distribution and ELFs from the RMC simulation agree well with Palik's data. In addition, different initial weighting factors with different initial values converge to the same value with small error and so does the band gap energy. This test proves that the final results are indeed independent of the initial trial inputs by the Markov chain property. It ensures that the optical properties can also be reasonably derived by this RMC method even without a proper choice of initial parameters (despite the in cost of longer simulation time).

ELFs of SiO_2 for 2000, 3000, and 4000 eV electrons are obtained together with an uncertainty range, which is determined by the maximum and the minimum values of the obtained ELFs at different emission angles, as shown in Fig. 11. The uncertainty range is smallest at 4000 eV, due to the smaller influence of surface excitations at higher energies. The mean value is then derived by averaging over all the ELFs for different energies and angles; Jin's data[19] derived from the same measured REELS spectra, but by a deconvolution procedure and Palik's data[76] are also shown in Fig. 11 for comparison. The present mean ELF agrees well with Palik's data except for the peak value and energy ~23 eV identified as the bulk plasmon and is also similar to Jin's data from the same REELS spectra. In previous work by Jin *et al.*,[19] the intensity of the bulk ELF was scaled by a factor of 1.22 that had been determined by fitting to the f-sum and ps-sum rules, while the present ELF is directly derived from REELS spectra without scaling. This result indicates that the ratio between elastic- and inelastic-scattering cross section is very well estimated when analyzing the REELS spectra. Furthermore, our obtained ELF contains finer features on the low energy-loss side of the main peak.

Optical constants can then be easily obtained from the bulk ELFs together with their uncertainty ranges. Fig. 12 presents the calculated reflective index n and extinction coefficient k of SiO_2 in the energy range of 9–60 eV. One can see a good agreement between our results and Palik's data,[76] especially for the refractive index n; the optical data from

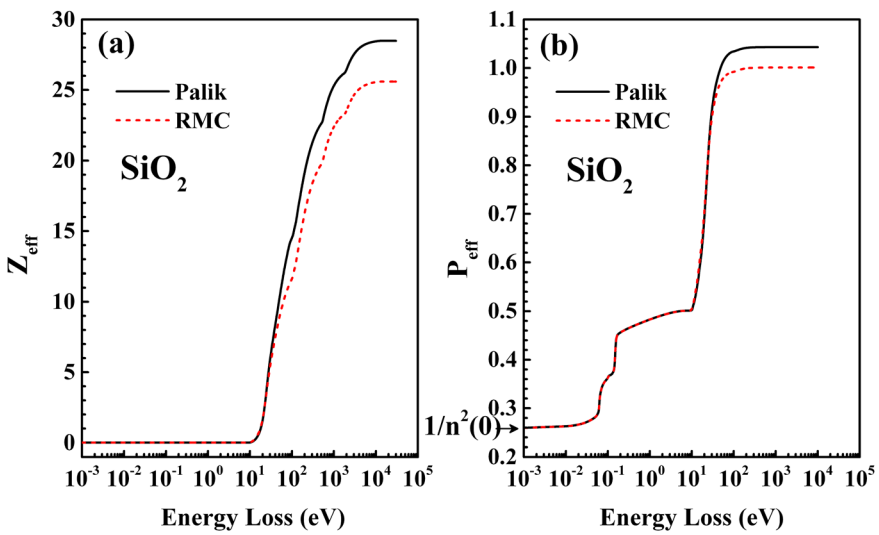

FIG. 13. Calculated results for the f-sum rule (a) and ps-sum rule (b) (dashed curves) for SiO_2 from the RMC method are compared with Palik's data (solid curves).

optical methods is within the present uncertainty range of our REELS analysis.

Sum rules were employed for checking the validity of the final ELF, the mean value of the ELFs obtained for different primary energies. It should be noted that the ELF we have determined here from REELS only concerns the energy loss range of 8–90 eV; hence, the present ELF data are used to take the place of relevant Palik's optical data in the photon energy range of 8–90 eV in evaluating oscillator strength (f-sum) and perfect-screening sum (ps-sum) rules.[4] Fig. 13(a) shows the effective number of electrons per molecule Z_{eff} as a function of energy loss. The calculated Z_{eff} is smaller than the expected value of 30 by 14.72%. Our result is smaller than the result from Palik's data[76] due to the lower peak intensity of our bulk ELF around ~23 eV. Fig. 13(b) shows the value of P_{eff} versus energy loss. For the ps-sum rule, $n(0)$ is the refractive index in the low-energy limit. The calculated P_{eff} including phonon-excitation effects is slightly larger than the expected unity by only 0.9%, which is better than the results for Palik's data where the deviation is 4.3%. This quantitative analysis shows that optical constants for the insulator SiO_2 are precisely obtained from REELS measurement using this RMC method.

V. CONCLUSIONS

A new theoretical method, the RMC method, is developed to deduce the bulk ELF and optical constants from REELS spectra. The method is based on the simulated annealing, i.e., MCMC sampling of oscillator parameters, weighting factors, and band gap energy, for deriving the bulk ELF used in a MC simulation of a REELS spectrum that agrees with an experimental spectrum. The bulk ELF and the dielectric function of SiO_2 are determined in the energy range of 8–90 eV by using the RMC method. The derived optical constants, the refractive index, and the extinction coefficient, show good agreement with Palik's data obtained from optical methods, indicating the reliability and applicability of the RMC method for obtaining the bulk ELF and optical properties from REELS measurements.

ACKNOWLEDGMENTS

This work was supported by the National Natural Science Foundation of China (Nos. 11074232, 11274288, and 11204289), the National Basic Research Program of China (Nos. 2011CB932801 and 2012CB933702), Ministry of Education of China (No. 20123402110034), and Strategic Japanese-Korean-Chinese Cooperative Program on Advanced Materials and Standards and "111" project. We thank the Supercomputing Center of USTC for support in performing parallel computations.

[1]Z. J. Ding, K. Salma, H. M. Li, Z. M. Zhang, K. Tokesi, D. Varga, J. Toth, K. Goto, and R. Shimizu, Surf. Interface Anal. **38**, 657 (2006).
[2]Z. J. Ding and R. Shimizu, Surf. Sci. **222**, 313 (1989).
[3]J. D. Bourke and C. T. Chantler, Phys. Rev. Lett. **104**, 206601 (2010).
[4]S. Tanuma, C. J. Powell, and D. R. Penn, Surf. Interface Anal. **11**, 577 (1988).
[5]S. Tanuma, C. J. Powell, and D. R. Penn, Surf. Interface Anal. **17**, 911 (1991).
[6]H. Shinotsuka, S. Tanuma, C. J. Powell, and D. R. Penn, Nucl. Instrum. Methods Phys. Res. B **270**, 75 (2012).
[7]C. J. Powell, J. Opt. Soc. Am. **59**, 738 (1969).
[8]C. J. Powell, J. Opt. Soc. Am. **60**, 78 (1970).
[9]C. J. Powell, J. Opt. Soc. Am. **60**, 214 (1970).
[10]S. Tougaard and I. Chorkendorff, Phys. Rev. B **35**, 6570 (1987).
[11]B. Dacison, *Neutron Transport Theory* (Oxford University Press, Oxford, 1955).
[12]W. S. M. Werner and M. Hayek, Surf. Interface Anal. **23**, 737 (1995).
[13]M. Vicanek, Surf. Sci. **440**, 1 (1999).
[14]W. S. M. Werner, Surf. Interface Anal. **22**, 79 (1994).
[15]Y. F. Chen, Phys. Rev. B **58**, 8087 (1998).
[16]H. Yoshikawa, R. Shimizu, and Z. J. Ding, Surf. Sci. **261**, 403 (1992).
[17]F. Yubero, S. Tougaard, E. Elizalde, and J. M. Sanz, Surf. Interface Anal. **20**, 719 (1993).
[18]W. Bekhti and M. Ghamnia, Catal. Today **89**, 303 (2004).
[19]H. Jin, H. Shinotsuka, H. Yoshikawa, H. Iwai, S. Tanuma, and S. Tougaard, J. Appl. Phys. **107**, 083709 (2010).
[20]H. Yoshikawa, T. Tsukamoto, R. Shimizu, and V. Crist, Surf. Interface Anal. **18**, 757 (1992).
[21]H. Yoshikawa, Y. Irokawa, and R. Shimizu, J. Vac. Sci. Technol. A **13**, 1984 (1995).
[22]L. Landau, J. Phys. (Moscow) **8**, 201 (1944).
[23]T. Nagatomi, Z. J. Ding, and R. Shimizu, Surf. Sci. **359**, 163 (1996).
[24]T. Nagatomi, R. Shimizu, and R. H. Ritchie, J. Appl. Phys. **85**, 4231 (1999).
[25]T. Nagatomi, R. Shimizu, and R. H. Ritchie, Surf. Sci. **419**, 158 (1999).
[26]Z. M. Zhang, T. Koshikawa, T. Iyasu, R. Shimizu, and K. Goto, Surf. Interface Anal. **35**, 403 (2003).
[27]Z. J. Ding, T. Nagatomi, R. Shimizu, and K. Goto, Surf. Sci. **336**, 397 (1995).
[28]Z. J. Ding and R. Shimizu, Scanning **18**, 92 (1996).
[29]Z. J. Ding and R. Shimizu, Phys. Rev. B **61**, 14128 (2000).
[30]Z. J. Ding, H. M. Li, Q. R. Pu, Z. M. Zhang, and R. Shimizu, Phys. Rev. B **66**, 085411 (2002).
[31]Z. J. Ding, H. M. Li, K. Goto, Y. Z. Jiang, and R. Shimizu, J. Appl. Phys. **96**, 4598 (2004).
[32]B. Da, S. F. Mao, G. H. Zhang, X. P. Wang, and Z. J. Ding, J. Appl. Phys. **112**, 034310 (2012).
[33]B. Da, S. F. Mao, G. H. Zhang, X. P. Wang, and Z. J. Ding, Surf. Interface Anal. **44**, 647 (2012).
[34]H. Jin, H. Shinotsuka, H. Yoshikawa, H. Iwai, M. Arai, S. Tanuma, and S. Tougaard, Surf. Interface Anal. **45**, 985 (2013).
[35]W. S. M. Werner, Phys. Rev. B **52**, 2964 (1995).
[36]W. S. M. Werner, Surf. Sci. **588**, 26 (2005).
[37]W. S. M. Werner, Surf. Interface Anal. **31**, 141 (2001).
[38]W. S. M. Werner, M. R. Went, and M. Vos, Surf. Sci. **601**, L109 (2007).
[39]W. S. M. Werner, K. Glantschnig, and C. Ambrosch-Draxl, J. Phys. Chem. Ref. Data **38**, 1013 (2009).
[40]N. Metropolis, A. W. Rosenbluth, M. N. Rosenbluth, A. H. Teller, and E. Teller, J. Chem. Phys. **21**, 1087 (1953).
[41]W. K. Hastings, Biometrika **57**, 97 (1970).
[42]S. Kirkpatrick, C. D. Gelatt, and M. P. Vecchi, Science **220**, 671 (1983).
[43]V. Cerny, J. Opt. Appl. **45**, 41 (1985).
[44]T. Kimura, S. Tanuma, M. Inoue, M. Suzuki, and T. Hashimoto, J. Surf. Anal. **9**, 75 (2002).
[45]K. Yanagiuchi, J. Surf. Anal. **1**, 395 (1995).
[46]N. F. Mott, Proc. R. Soc. London A **124**, 425 (1929).
[47]Z. Czyzewski, D. O. MacCallium, A. Romig, and D. C. Joy, J. Appl. Phys. **68**, 3066 (1990).
[48]R. A. Bonham and T. G. Strand, J. Chem. Phys. **39**, 2200 (1963).
[49]A. Jablonski, F. Salvat, and C. J. Powell, J. Phys. Chem. Ref. Data **33**, 409 (2004).
[50]S. Tanuma, T. Shiratori, T. Kimura, K. Goto, S. Ichimura, and C. J. Powell, Surf. Interface Anal. **37**, 833 (2005).
[51]Z. J. Ding, Phys. Rev. B **55**, 9999 (1997).
[52]Z. J. Ding, J. Phys.: Condens. Matter **10**, 1733 (1998).
[53]Z. J. Ding, J. Phys.: Condens. Matter **10**, 1753 (1998).
[54]G. Chiarello, E. Colavita, M. D. Crescenzi, and S. Nannarone, Phys. Rev. B **29**, 4878 (1984).
[55]E. Colavita, M. D. Crescenzi, L. Papagno, R. Scarmozzino, L. S. Caputi, R. Rosei, and E. Tossati, Phys. Rev. B **25**, 2490 (1982).

[56]M. D. Crescenzi, E. Colavita, L. Papagno, G. Chiarello, R. Scarmozzino, L. S. Caputi, and R. Rosei, J. Phys. F **13**, 895 (1983).
[57]Y. F. Chen and Y. T. Chen, Phys. Rev. B **53**, 4980 (1996).
[58]Y. F. Chen and C. M. Kwei, Surf. Sci. **364**, 131 (1996).
[59]Y. C. Li, Y. H. Tu, C. M. Kwei, and C. J. Tung, Surf. Sci. **589**, 67 (2005).
[60]B. Da, S. F. Mao, and Z. J. Ding, J. Phys.: Condens. Matter **23**, 395003 (2011).
[61]J. C. Ashley, J. Electron Spectrosc. Relat. Phenom. **46**, 199 (1988).
[62]R. H. Ritchie and A. Howie, Philos. Mag. A **36**, 463 (1977).
[63]C. M. Kwei, Y. F. Chen, C. J. Tung, and J. P. Wang, Surf. Sci. **293**, 202 (1993).
[64]D. P. Landau and K. Binder, *A Guide to Monte Carlo Simulations in Statistical Physics* (Cambridge University Press, Cambridge, 2000).
[65]M. H. Reilly, J. Phys. Chem. Solids **31**, 1041 (1970).
[66]K. L. Yip and W. B. Fowler, Phys. Rev. B **10**, 1400 (1974).
[67]S. T. Pantelides, Phys. Lett. A **54**, 401 (1975).
[68]P. M. Schneider and W. B. Fowler, Phys. Rev. Lett. **36**, 425 (1976).
[69]C. E. Moore, in *Atomic Energy Levels, U. S. National Bureau of Standards, National Standard Reference Data Systems* (U. S. GPO, Washington, DC, 1971), Vol. 35.
[70]T. H. DiStefano and D. E. Eastman, Solid State Commun. **9**, 2259 (1971).
[71]F. Aryasetiawan and O. Gunnarsson, Rep. Prog. Phys. **61**, 237 (1998).
[72]L. E. Ramos, J. Furthmuller, and F. Bechstedt, Phys. Rev. B **69**, 085102 (2004).
[73]B. Da, Y. Sun, S. F. Mao, and Z. J. Ding, Surf. Interface Anal. **45**, 773 (2013).
[74]A. Barranco, F. Yubero, J. P. Espinos, P. Groening, and A. R. Gonzalez-Elipe, J. Appl. Phys. **97**, 113714 (2005).
[75]J. Park, S. Heo, J. G. Chung, H. Kim, H. Lee, K. Kim, and G. S. Park, Ultramicroscopy **109**, 1183 (2009).
[76]E. D. Palik, *Handbook of Optical Constants of Solids* (Academic, Orlando, FL, 1985).